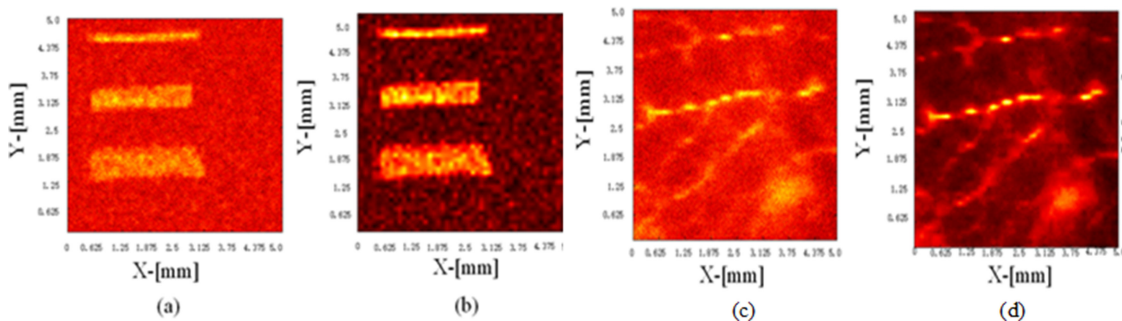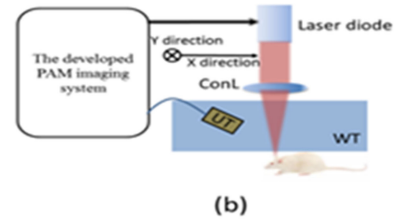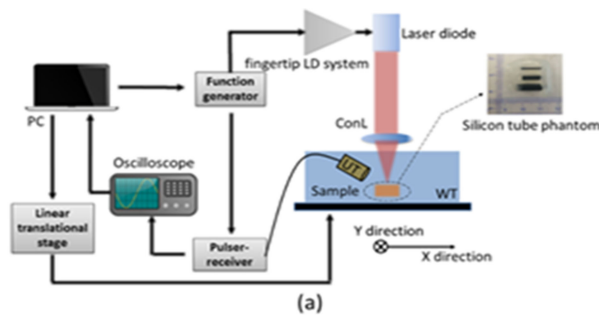# A Noise Reduction Method for Photoacoustic Imaging *In Vivo* Based on EMD and Conditional Mutual Information

Meng Zhou
Haibo Xia
Hongtao Zhong
Jiayao Zhang
Fei Gao, *Member, IEEE*

A Noise Reduction Method for Photoacoustic Imaging *In Vivo* Based on EMD and Conditional Mutual Information

Meng Zhou,[1,2,3] **Haibo Xia,**[1,2,3] **Hongtao Zhong,**[2,3] **Jiayao Zhang,**[2] **and Fei Gao** [2] *Member, IEEE*

[1]Chinese Academy of Sciences, Shanghai Advanced Research Institute, Shanghai 201210, China
[2]Hybrid Imaging System Laboratory, School of Information Science and Technology, ShanghaiTech University, Shanghai 201210, China
[3]University of Chinese Academy of Sciences, Beijing 100049, China

Abstract: Photoacoustic tomography is a technique to reconstruct the image of light energy absorption distribution in tissues based on the detected photoacoustic signals. In recent years, this research field has been greatly developed, and its application range is wide, including anatomy, functionality, and molecular imaging. However, the conversion efficiency of photoacoustic effect from light to sound is quite low, which leads to the low signal-to-noise ratio of photoacoustic signal and the poor quality of reconstructed photoacoustic image. The traditional method to improve the signal-to-noise ratio of photoacoustic signals is data averaging method, but it seriously limits the imaging speed due to multiple acquisition. Without sacrificing signal fidelity and imaging speed, an empirical mode decomposition (EMD) combined with conditional mutual information de-noising algorithm for photoacoustic tomography is proposed in this paper. The simulation results and experimental results of photoacoustic signal de-noising achieve significant improvement of signal-to-noise ratio of photoacoustic signal and the enhancement of contrast of the reconstructed image. The simulation results and experimental results show that EMD combined with mutual information method improves at least 2 dB and 3 dB, respectively, more than traditional wavelet threshold method and band-pass filter. The improvement of contrast-to-noise ratio is more than 2 dB and 3 dB, respectively, more than traditional wavelet threshold method and band-pass filter.

Index Terms: Empirical mode decomposition, Mutual information, Noise reduction algorithm, Photoacoustic signal simulation, Signal-to-noise ratio.

1. Introduction

Photoacoustic (PA) imaging has been widely used in anatomical, functional and molecular imaging because it breaks the limitation of light diffusion in deep penetration [1]–[7]. At the larger end, PA imaging has been reported for whole-body animal imaging [8], four dimensional (4D) epilepsy detection [9], and real-time three dimensional (3D) visualization of human vasculature [10], At the small scale, PA microscopy [11], and mesoscopic imaging had been reported for micro-vasculature

mapping, temperature measurement of a single cell [12], skin layer visualization and skin cancer imaging [13].

However, there is an open challenge that the conversion efficiency of photoacoustic effect from light to sound is quite low, which leads to the low signal-to-noise ratio (SNR) of PA signal and the poor quality of reconstructed photoacoustic image especially. Great effort has been made to reduce the noise in PA imaging. The most common method to improve the SNR of PA signal is data averaging, but it is time-consuming method due to multiple data acquisition. Low-pass or band-pass filter is also used to increase SNR of PA signal and remove the noise, which is useless when signal and noise share similar frequency spectrum. Besides, band-pass filter may seriously distort the original photoacoustic signal while reducing noise. Different wavelet de-noising methods have been studied in pervious literatures. These methods both have to choose the appropriate wavelet basis function and the number of wavelet decomposition level according to the frequency component and sampling frequency of the signals to achieve good noise reduction effect [14]–[17], which can not achieve automatic signal noise reduction. [18]. Singular Value decomposition (SVD) was used to identify and remove laser-induced noise [19], but it's only useful to reduce laser-induced noise. Basis pursuit deconvolution is proposed, which is used to improve model-based reconstructed images [20]. The improvement is not particularly obvious. There is also literature where empirical mode decomposition (EMD) is used to decompose the spectral contributions of different photo-absorbing molecules of interest in multispectral optoacoustic tomography [21].

Improving the SNR of photoacoustic signal effectively is essential for improving the quality of photoacoustic image. Empirical mode decomposition (EMD) takes advantage of the time scale characteristics of data itself. It is quite suitable for non-stationary and non-linear physiological signals such as photoacoustic signals [22]. Therefore, EMD is widely used in many signal-processing fields [23]–[25]. In the case of noisy PA signal, EMD adaptively decomposes PA signal into a number of intrinsic mode function (IMF), and then select some IMF as the approximated noise signal. Therefore, an effective measurement is needed to select IMF. In literature [26], mutual information is used for feature selection. Mutual information is the amount of information shared between two or more random variables. Our proposition is to use mutual information to choose appropriate IMFs.

In this paper, we firstly use EMD to decompose the PA signal into IMFs, and then use mutual information as the criterion to determine the IMFs that need to be de-noised. These IMFs are de-noised by unbiased risk estimation minimization method. After de-noising, the clean photoacoustic signal is obtained and the final de-noised photoacoustic image is obtained. The simulation and experimental images verify that the performance of our noise reduction method is better than unbiased risk estimation wavelet threshold de-noising method and band-pass filter de-noising method.

2. Theory

2.1 Empirical Mode Decomposition

EMD is an adaptive signal decomposition method, which extracts the IMFs from the original signal by using the time scale characteristics of the signal itself, and finally obtains the spectrum with physical significance. At any point in time, data generally contain multiple fluctuation patterns. Given a signal, after EMD processing, several IMFs and residual signals will be obtained. IMF is required to satisfy two conditions. One is the number of extremes (maxima and minima) and zero crossings must either be equal or differ at most by one [27]. Another is the envelope of the local maximum (upper envelope) and the envelope of the local minimum (lower envelope) must be zero on average. It is used to characterize the frequency characteristics of data. The decomposition process of extracting IMF components is as follows [28]:

1) Determine all the maximum and minimum points in the original signal.
2) Cubic spline interpolation is used to fit the upper envelope and the lower envelope Respectively.
3) Calculating the local average of the upper and lower envelopes.

4) Subtracting the local average from the upper and lower envelopes, the low frequency components can be removed.

Repeating steps (1)–(4) until the two conditions of IMF are finally satisfied. Once an IMF is generated, the residue of signal is treated as the original signal, and the repetition of step (1)–(4) generates a new IMF and the final residue. After such an iteration process, a finite number of IMFs and residuals whose final amplitude and frequency are approximately zero are obtained. Each IMF component reflects the characteristic scale of the signal and represents the intrinsic modal characteristics of the non-linear and non-stationary signal. The noise of the original signal is mainly contained in a limited number of IMFs, and these IMFs can be effectively selected by measuring indicators.

2.2 Mutual Information Theory

After EMD, the original signal is decomposed into a finite number of IMFs and residues. The next step is to select some IMFs as approximations of noise signals in the original signal. Mutual information is the amount of information shared between two or more random variables. The main goal of feature selection is to use as few variables to carry as much information as possible in order to remove irrelevant and redundant variables. In practice, the former IMFs are mainly high-frequency information and carry more noise. Therefore, it is proposed to calculate the mutual information between each of the first half of the IMF and the sum of the second half of the IMFs. The original signal is initially partitioned, and the initial partition index (I) is [nm/2], where nm is the total number of IMFs. The IMFs whose index is less than or equal to I are set as the initial high frequency group, and the remaining IMF was set as the initial low frequency group. When an IMF carries more unknown useful signals and less noise information, it is better to express original useful signals. According to this principle, by minimizing the mutual information between the selected IMF and the noisy PA signal, the selected mode has the most useful information. Mutual information based feature selection adds current variables to the set of variables that have been selected. We minimize the following:

$$MI(y, \hat{x}) - \sum_{x_j \in \phi} MI(\hat{x}, x_j) \tag{1}$$

where y is the noisy signal, $\hat{x}$ is the IMF to be selected, and x_j is the set of IMFs that have been selected. MI represents the mutual information between them.

2.3 De-Noising Process

For the variable selection problem of IMFs, the target is to choose a set of IMFs to minimize formula (1) and to find a large number of noisy IMFs. Then do de-noising processing to this IMFs. Finally reconstruct the original useful signal. The flow is divided into four steps:

1) The original noisy signal is decomposed by EMD, and a limited number of IMFs and residues are obtained.
2) The obtained IMF is divided into high-frequency groups, which assume that the low-frequency combination contains a large number of useful signals and a large number of noise signals.
3) The final low-frequency group and high-frequency group are calculated by mutual information theory.
4) Stein's unbiased risk estimate (SURE) threshold de-noising process is applied to the high frequency group. Its form is as follows:

$$SURE_{EMD} = N - 2 \times Q\left(j : |d_{j,k}| \leq \lambda\right) + \sum_{j=1}^{N} \sum_{k=1}^{K-1} \left(|d_{j,k}| \wedge \lambda\right)^2 \tag{2}$$

where λ is alternative threshold, $a \wedge b$ denote $\min(a, b)$, $d_{j,k}$ is high-frequency group, N is the points of data, and Q is the number less than λ. After the final threshold is obtained by minimizing (1), we
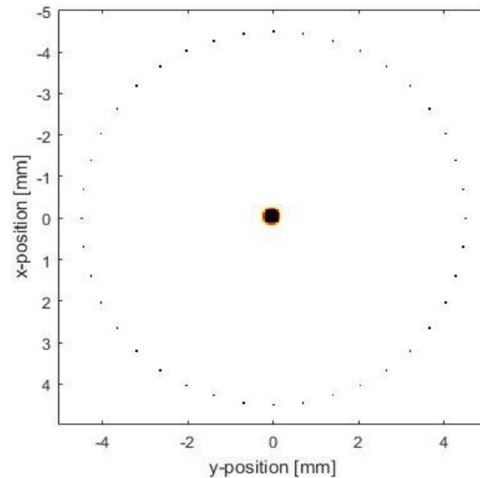
Fig. 1. Illustration of geometry used in numerical simulation.

use the hard threshold process to do de-noising. The form of the hard threshold is as follows:

$$\bar{d}_{j,k} = \begin{cases} d_{j,k}, & |d_{j,k}| \geq \lambda \\ 0, & |d_{j,k}| \geq \lambda \end{cases} \qquad (3)$$

5) Accumulating the high frequency IMF group and the low frequency IMF group after noise reduction is to obtaining the final noise reduction signal.

3. Numerical Simulation

3.1 Simulation Setup and Metrics

Through the K-wave tool in MATLAB, the simulated photoacoustic signals can be generated and propagating in 2D [29]. The simulation settings are shown in Fig. 1.

A 40 mm square grid is created and 40 detectors with 700 μm spacing are used to detect photoacoustic signals. The received photoacoustic signals are normalized according to the global maximum amplitude of the received signals of the 40 detectors. In order to effectively evaluate the performance of different noise reduction methods, an effective scale disk absorber is used. Five different levels of noise (signal-to-noise ratio is -3 dB, -5 dB, -7 dB, -9 dB, -11 dB) are added to the original simulated clean photoacoustic signal. The signal-to-noise ratio of noise is calculated by the following formula:

$$\text{SNR} = 20\log\left(\left(\sqrt{\text{mean}\,(n(t))}\right)^2 / \max\,(s(t))\right) \qquad (4)$$

where $s(t)$ is the clean photoacoustic signal, $n(t)$ is the added noise signal, $\max(s(t))$ is the largest value of the clean signal, $\text{mean}(n(t))$ is the average amplitude of the noise signal. In this paper, the EMD and mutual information de-noising method, the traditional wavelet threshold de-noising method and band-pass filtering method are compared. For the selection of the basis function and decomposition layer of the wavelet threshold de-noising method, the commonly used wavelet basis function family (Harr wavelet family, Daubechies wavelet family, Symlet wavelet family) are selected to compare the de-noising effect. According to the SNR after de-noising, the Symlet 6 wavelet is selected for six-level decomposition [30]. For the threshold selection of wavelet threshold de-noising, the most commonly used unbiased risk estimation threshold (rigrsure threshold) is used [31]. The low frequency cut-off frequency and high frequency cut-off frequency of band-pass filter
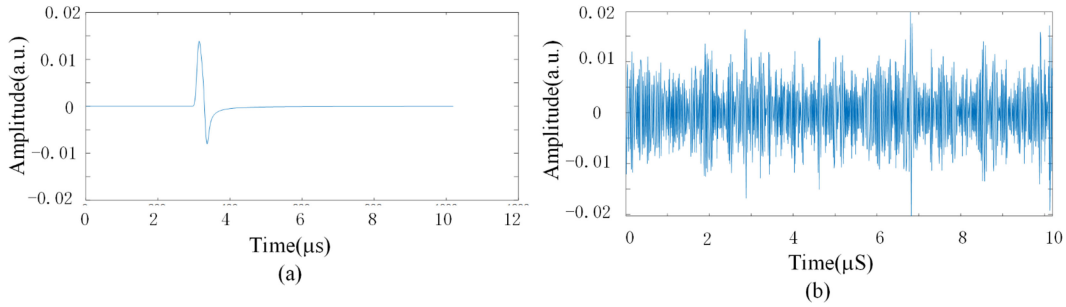
Fig. 2. (a) Simulate the photoacoustic clean signal. (b) Add −5 dB noise signal.

are 3 MHZ and 7 MHZ respectively. The photoacoustic signal after noise reduction is obtained by the above three methods.

In order to evaluate the effect of noise reduction under different methods, SNR and normalized cross correlation (NCC) of curve similarity parameters are selected as comparison parameters. Clean and useful signals can be regarded as a standard signal. The SNR of de-noised signals obtained from noisy noises is defined as the following:

$$\text{SNR} = 10 \log \left[\frac{\sum_n s^2(n)}{\sum_n [\hat{s}(n) - s(n)]^2} \right] \tag{5}$$

NCC is used to evaluate the similarity between clean and useful signals and de-noised signals. It is defined as follows:

$$\text{NCC} = \sum_n s(n)\hat{s}(n) \Big/ \sqrt{\left(\sum_n \left(s^2(n) \right) \sum_n \left(\hat{s}^2(n) \right) \right)} \tag{6}$$

For reconstructed images, the relative contrast-to-noise ratio (CNR) can be used to measure [32].

$$\text{CNR} = 20 \log \left(\frac{|s_i - s_o|}{\sqrt{\sigma_o^2}} \right) \tag{7}$$

where s_i and s_o are the average brightness inside and outside the imaging target respectively, and σ_o is the variance outside the imaging target.

3.2. Noise Reduction Simulation Results

When the typical noise level is −5 dB, the original clean signal and the noisy signal are shown in Fig. 2.

We can see that the photoacoustic signal is basically submerged in the noise when the noise level is −5 dB. At this time, an effective noise reduction method is needed to extract useful photoacoustic signals. Three methods are used to de-noise the simulated noisy signal, and the de-noising results in Fig. 3 are obtained.

Fig. 3 shows the de-noising results of three methods for noisy signals. Three methods are EMD combined with mutual information de-noising method, Unbiased risk estimation wavelet threshold de-noising method and Band-pass filter de-noising method. Observing the results of noise reduction, EMD combined with mutual information is better than the other two traditional methods. In Fig. 4, the noise reduction effect of these three methods are quantitatively compared under different noise levels. EMD combined with mutual information method improves 5 dB and 7 dB respectively more than traditional wavelet threshold method and band-pass filter when the noisy level is −3 dB.

As expected, all methods improve SNR and NCC. At −5 dB noise level, EMD combined with mutual information method improves 4 dB and 6 dB respectively more than traditional wavelet
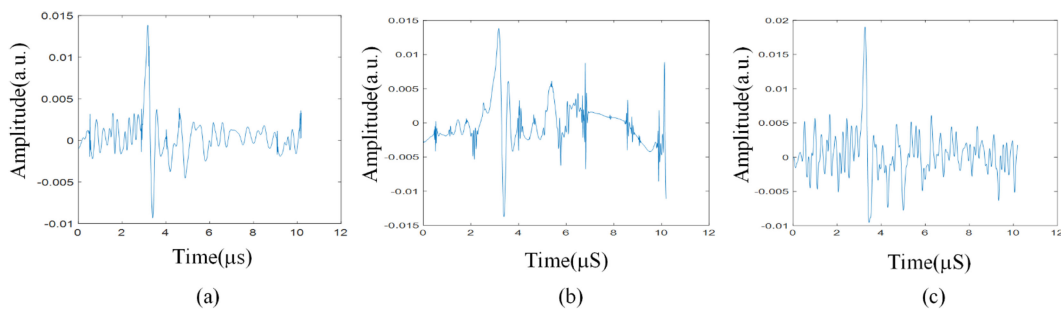
Fig. 3. The de-noising results of simulation photoacoustic signal de-noising (a) EMD combined with mutual information de-noising method. (b) Unbiased risk estimation wavelet threshold de-noising method (c) Band-pass filter de-noising method.
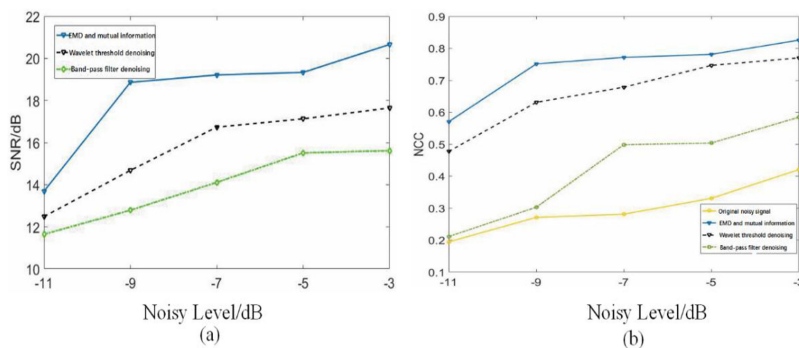

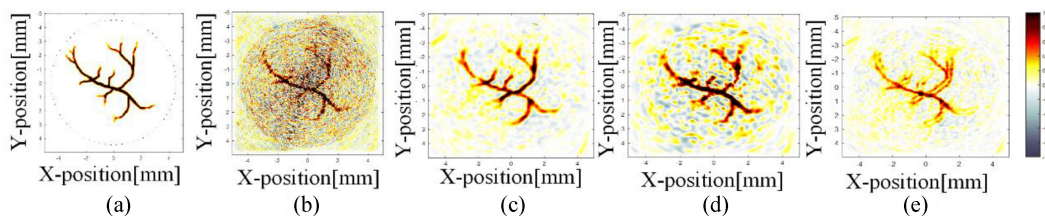Fig. 4. Comparison of three methods in terms of (a) SNR, (b) NCC.

Fig. 5. Constructed de-noising image results of PA image when simulation signal SNR is 5 dB for three methods: (a) Original simulation PA image, (b) Noisy image SNR = 5 dB, (c) EMD combined with mutual information de-noising method, (d) Unbiased risk estimation wavelet threshold de-noising method, (f) Band-pass filter de-noising method.

TABLE 1

Simulation Vessel Image Comparing Three Methods

Image metric	Original image	EMD combined Mutual Information	Wavelet Threshold	Band-pass filter de-noising
CNR(dB)	5.3	19.8	15.6	14.5

threshold method and band-pass filter. Therefore, EMD combined with mutual information de-noising method has enhanced de-noising performance for photoacoustic signals with high noise level. We also use a simulated blood vessel image to verify our method. Fig. 5. shows the simulated image reconstruction results when the noisy level is −5 dB. We also use Table 1 to show the CNR of three de-noising methods.
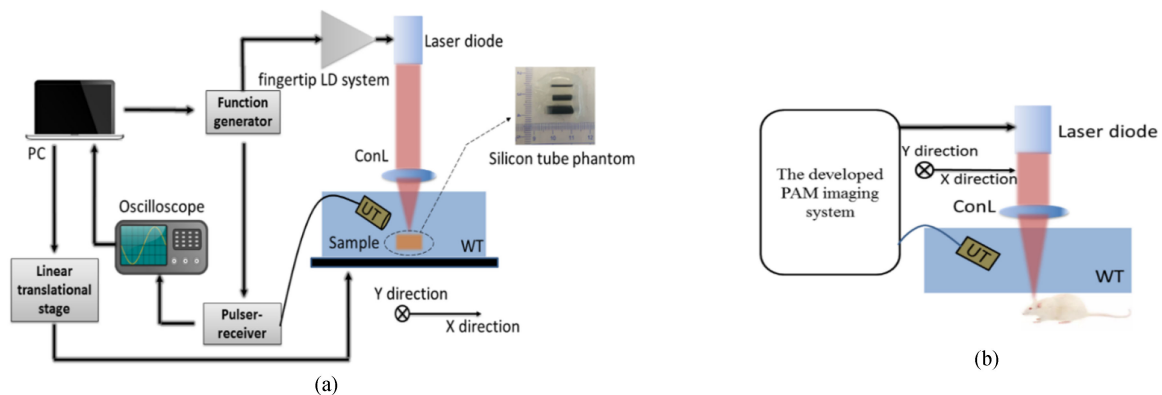
Fig. 6. Schematic imaging setup. PC: personal computer; UT: ultrasound transducer; WT: water tank; LD: laser diode, (a) photoacoustic microscopy (PAM) system tube phantom setup, (b) mouse ear imaging setup.

4. Experimental in Vivo Mice Ear Blood Vessel and Phantom Results

4.1 Experimental Setup

Here, we developed a photoacoustic microscopy (PAM) system (Fig. 6(a)) for two-dimensional imaging. The raster scan was achieved by the linear translational stage controlled by a personal computer (PC) to tune the position of the water tank in the x-y plane. The imaging area was about 20 mm × 20 mm, and scan step size was 0.4 mm. The function generator outputs pulse signals with 40 ns laser pulse width with 1 KHz repetition rate. The laser was weakly focused to be about 500 μm spot size by a condenser lens (100 mm focal length). The phantom consisted of three silicon tubes filled with ink with different inner diameter (1 mm, 2 mm and 3 mm), and the effective length was about 10 mm. The generated PA signals were received by an immersion focused ultrasound transducer (I10C8F20, Doppler Inc.) with 10 mm diameter and 10 MHz central frequency. The pulser-receiver (5072PR, Olympus) was used to amplify the PA signals with 45 dB gain. The signals in time-domain and frequency-domain imaging were acquired using an oscilloscope (DPO5204B, Tektronix Inc.) by averaging 256 times and transferred to PC.

To further validate our method in vivo PA imaging, a ten-weeks-old mouse has also been prepared. All procedures were approved by the Animal Care Committee of ShanghaiTech University School of Life Science and Technology. The mouse was anesthetized with 2% vaporized isoflurane through the experiments. One of the ears was selected to be served as the imaging objects. The imaging setup was shown in Fig. 6(b). The laser spot was further focused to be about 200 μm and the scan step size is 100 μm. The pulse width was set to be 200 ns for time-domain imaging and the chip frequency was 1–3 MHz with duration of 100 μs for frequency-domain imaging. The imaging area was about 5 mm × 5 mm. The laser was moved point by point under the control of the linear translational stage. The generated PA signal was coupled to the ultrasound transducer by the medical ultrasonic coupling agent, plastic wrap, and water. Other system setting of in vivo imaging was the same as that of the silicon tube phantom experiment mentioned above.

4.2 Experimental result

The results of the three de-noising methods are shown in Figs. 7 and 8.

The CNR of three de-noising methods also shows in Table II.

We can see that EMD combined mutual Information de-noising method has the highest CNR. Moreover, EMD combined mutual Information de-noising method realizes the automatic decomposition and noise reduction, which does not require the selection of parameters.
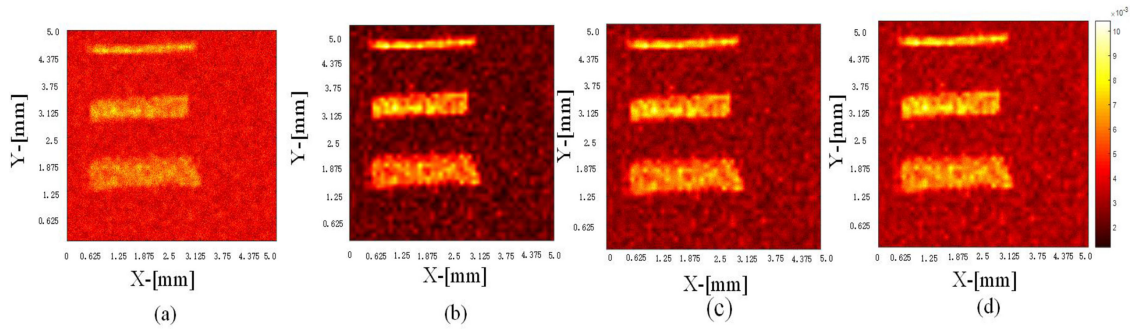
Fig. 7. MAP image of tube phantom and de-nosing images\ (a) Original MAP image, (b) EMD combined with mutual information de-noising method, (c) Unbiased risk estimation wavelet threshold de-noising method, (d) Band-pass filter de-noising method.

Fig. 8. MAP image of the mice ear blood vessel and de-nosing images in vivo (a) Original MAP image, (b) EMD combined with mutual information de-noising method, (c) Unbiased risk estimation wavelet threshold de-noising method, (d) Band-pass filter de-noising method.
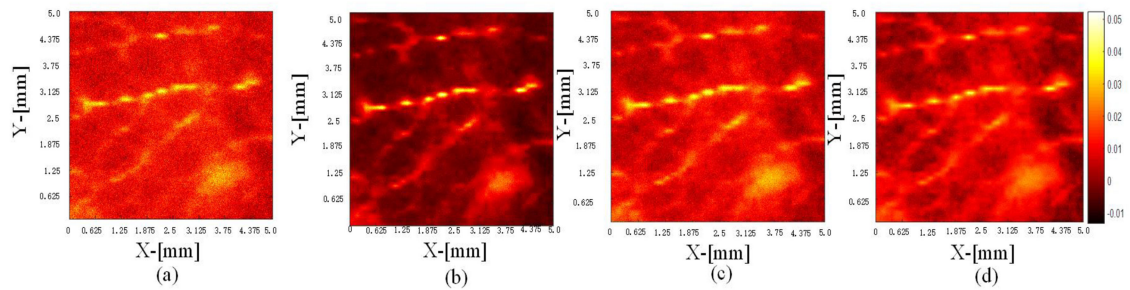
TABLE II
Mice Ear Vessel Image Comparing Three Methods

Image metric CNR(dB)	Original image	EMD combined Mutual Information	Wavelet Threshold	Band-pass filter de-noising
Tube phantom	8.5	27.7	25.2	24.9
Mice ear	4.7	21.5	16.3	18.2

5. Conclusion

In this paper, an EMD method combining mutual information de-noising method is proposed. This method is based on the hypothesis of high frequency IMFs group with a lot of noise and low frequency IMFs group with a lot of useful signals. High frequency IMFs group and low frequency IMFs group can be effectively obtained by mutual information. Then, only shrinkage threshold is applied to de-noise the high-frequency IMFs group. When choosing threshold, SURE threshold that is often used in discrete wavelet transform is adopted. SURE does not need to estimate the noise of the original noisy signal. When the original signal is unknown, it can estimate the real mean square error well. When validating the effectiveness of the method, the method is applied to reduce the noise of the simulated photoacoustic signal and in vivo mice ear blood vessel imaging. The proposed method is compared with other two conventional methods. The simulation results and experimental results show EMD combined with mutual information method improves at least 2 dB and 3 dB respectively more than traditional wavelet threshold method and band-pass filter. The improvement

of CNR is more than 2 dB and 3 dB respectively more than traditional wavelet threshold method and band-pass filter The results show that this method can effectively eliminate the noise in the photoacoustic signal while retaining the useful signal characteristics. The image recovered by this method has higher SNR and contrast. With the further development of this algorithm, it can greatly improve the SNR and image quality of PA signals, thus providing potential development for low-cost real-time photoacoustic imaging systems.

References

[1] L. V. Wang and S. Hu, "Photoacoustic tomography: *In Vivo* imaging from organelles to organs," *Science*, vol. 335, no. 6075, pp. 1458–1462, 2012, doi: 10.1126/science.1216210.

[2] D. Razansky *et al.*, "Multispectral opto-acoustic tomography of deep-seated fluorescent proteins in vivo," *Nature Photon.*, vol. 3, pp. 412–417, 2009.

[3] G. Fei, F. Xiaohua, and Z. Yuanjin, "Advanced photoacoustic and thermoacoustic sensing and imaging beyond pulsed absorption contrast," *J. Opt.*, vol. 18, no. 7, 2016, Art. no. 074006.

[4] L. V. Wang, "Tutorial on photoacoustic microscopy and computed tomography," *IEEE J. Sel. Topics Quantum Electron.*, vol. 14, no. 1, pp. 171–179, Jan./Feb. 2008.

[5] F. Gao *et al.*, "Single laser pulse generates dual photoacoustic signals for differential contrast photoacoustic imaging," *Sci. Rep.*, vol. 7, no. 1, 2017, Art. no. 626.

[6] J. Zhang, B. Chen, M. Zhou, H. Lan, and F. Gao, "Photoacoustic image classification and segmentation of breast cancer: A feasibility study," *IEEE Access*, vol. 7, pp. 5457–5466, 2019.

[7] H. Lan, T. Duan, H. Zhong, Z. Meng, and G. Fei, "Photoacoustic classification of tumor model morphology based on support vector machine: A simulation and phantom study," *IEEE J. Sel. Topics Quantum Electron.*, vol. 25, no. 1, Jan./Feb. 2018, Art. no. 7201409.

[8] J. Xia *et al.*, "Whole-body ring-shaped confocal photoacoustic computed tomography of small animals in vivo," *J. Biomed. Opt.*, vol. 17, 2012, Art. no. 050506.

[9] L. Xiang, B. Wang, L. Ji, and H. Jiang, "4-D Photoacoustic Tomography," *Scientific Rep.*, vol. 3, 2013, Art. no. 1113.

[10] E. Z. Zhang, J. G. Laufer, R. B. Pedley, and P. C. Beard, "In vivo high-resolution 3D photoacoustic imaging of superficial vascular anatomy," *Phys. Med. Biol.*, vol. 54, no. 4, 2009, Art. no. 1035.

[11] K. Maslov, H. F. Zhang, S. Hu, and L. V. Wang, "Optical-resolution photoacoustic microscopy for in vivo imaging of single capillaries," *Opt. Lett.*, vol. 33, no. 9, pp. 929–931, 2008.

[12] L. Gao *et al.*, "Single-cell photoacoustic thermometry," *J. Biomed. Opt.*, vol. 18, 2018, Art. no. 26003.

[13] L. V. Wang, "Multiscale photoacoustic microscopy and computed tomography," *Nature Photon.*, vol. 3, pp. 503–509, 2009.

[14] J. A. Viator, B. Choi, M. Ambrose, J. Spanier, and J. S. Nelson, "In vivo port-wine stain depth determination with a photoacoustic probe," *Appl. Opt.*, vol. 42, no. 16, pp. 3215–3224, 2003.

[15] H. H. Scott and A. V. John, "Automated wavelet denoising of photoacoustic signals for circulating melanoma cell detection and burn image reconstruction," *Phys. Med. Biol.*, vol. 53, no. 12, p. N227–N236, 2008.

[16] S. A. Ermilov *et al.*, "Laser optoacoustic imaging system for detection of breast cancer," *J. Biomed. Opt.*, vol. 14, 2009, Art. no. 024007.

[17] M. Zhou, H. Xia, H. Lan, T. Duan, H. Zhong, and F. Gao, "Wavelet de-noising method with adaptive threshold selection for photoacoustic tomography," in *Proc. 40th Ann. Int. Conf. IEEE Eng. Med. Biol. Soc.*, 2018, pp. 4796–4799.

[18] I. K. Otchere, D. O. Ampofo, and E. A. Frimpong, "Adaptive discrete wavelet transform based technique for load frequency control," in *Proc. IEEE PES PowerAfrica*, 2017, pp. 589–594.

[19] E. R. Hill, W. Xia, M. J. Clarkson, and A. E. Desjardins, "Identification and removal of laser-induced noise in photoacoustic imaging using singular value decomposition," *Biomed. Opt. Exp.*, vol. 8, no. 1, pp. 68–77, 2017.

[20] J. Prakash, A. S. Raju, C. B. Shaw, M. Pramanik, and P. K. Yalavarthy, "Basis pursuit deconvolution for improving model-based reconstructed images in photoacoustic tomography," *Biomed. Opt. Exp.*, vol. 5, no. 5, pp. 1363–1377, 2014.

[21] G. Jürgen, N. C. Deliolanis, B. Andreas, R. Daniel, and N. Vasilis, "Blind source unmixing in multi-spectral optoacoustic tomography," *Opt. Exp.*, vol. 19, no. 4, pp. 3175–3184, 2011.

[22] L. Hualou, L. Qiu-Hua, and J. D. Z. Chen, "Application of the empirical mode decomposition to the analysis of esophageal manometric data in gastroesophageal reflux disease," *IEEE Trans. Biomed. Eng.*, vol. 52, no. 10, pp. 1692–1701, Oct. 2005.

[23] Y. Lei, L. Jing, Z. He, and M. J. Zuo, "A review on empirical mode decomposition in fault diagnosis of rotating machinery," *Mech. Syst. Signal Process.*, vol. 35, no. 1/2, pp. 108–126, 2013.

[24] N. U. Rehman and D. P. Mandic, "Filter bank property of multivariate empirical mode decomposition," *IEEE Trans. Singal Procees.*, vol. 59, no. 5, pp. 2421–2426, May 2011.

[25] J. C. Echeverría, J. A. Crowe, M. S. Woolfson, and B. R. Hayes-Gill, "Application of empirical mode decomposition to heart rate variability analysis," *Med. Biol. Eng. Comput.*, vol. 39, no. 4, pp. 471–479, 2001.

[26] F. Fleuret, "Fast binary feature selection with conditional mutual information," *J. Mach. Learn. Res.*, vol. 5, pp. 1531–1555, 2004.

[27] N. u. Rehman and D. P. Mandic, "Empirical mode decomposition for trivariate signals," *IEEE Trans. Signal Process.*, vol. 58, no. 3, pp. 1059–1068, 2010.

[28] P. Flandrin, G. Rilling, and P. Goncalves, "Empirical mode decomposition as a filter bank," *IEEE Signal Process. Lett.*, vol. 11, no. 2, pp. 112–114, 2004.

[29] B. E. Treeby and B. T. Cox, "k-Wave: MATLAB toolbox for the simulation and reconstruction of photoacoustic wave fields," *J. Biomed. Opt.*, vol. 15, 2010, Art. no. 021314.

[30] U. Seljuq, F. Himayun, and H. Rasheed, "Selection of an optimal mother wavelet basis function for ECG signal denoising," in *Proc. 17th IEEE Int. Multi Topic Conf.*, 2014, pp. 26–30.

[31] D. Valencia, D. Orejuela, J. Salazar, and J. Valencia, "Comparison analysis between rigrsure, sqtwolog, heursure and minimaxi techniques using hard and soft thresholding methods," in *Proc. 21st Symp. Signal Process., Images Artif. Vis.*, 2016, pp. 1–5.

[32] M. K. Karaaslan, G. Ö, N. Muzoğlu, and M. A. Arıcı, "Variation of contrast-noise ratio (CNR) and mean glanduler dose according to breast thickness," in *Proc. 20th Nat. Biomed. Eng. Meeting*, 2016, pp. 1–4.